Desalination and Water Treatment
www.deswater.com
doi: 10.1080/19443994.2014.989918

57 (2016) 4110–4121
February

Taylor & Francis
Taylor & Francis Group

Fe_3O_4 nanoparticles loaded onto wheat straw: an efficient adsorbent for Basic Blue 9 adsorption from aqueous solution

Azadeh Ebrahimian Pirbazari*, Elham Saberikhah, Nima Gholami Ahmad Gorabi

Faculty of Fouman, College of Engineering, University of Tehran, P.O. Box 43515-1155, Fouman 43516-66456, Iran, Tel. +98 1327234927; Fax: +98 1327237228; emails: aebrahimian@ut.ac.ir (A. Ebrahimian Pirbazari), esaberikhah@ut.ac.ir (E. Saberikhah), nima_gholami@ut.ac.ir (N. Gholami Ahmad Gorabi)

Received 24 May 2014; Accepted 14 November 2014

ABSTRACT

The adsorption of Basic Blue 9 (BB9) from aqueous solution by Fe_3O_4 nanoparticles loaded onto wheat straw (NP-WS) from agricultural biomass was investigated. Magnetic nanoparticles (Fe_3O_4) were prepared by chemical precipitation of a Fe^{2+} and Fe^{3+} salts from aqueous solution by ammonia. These nanoparticles of the adsorbent were characterized by field emission scanning electron microscopy, X-ray diffraction, Fourier transform infrared spectroscopy and nitrogen physisorption. The adsorption isotherm data were fitted to Langmuir, Sips, Redlich–Peterson, and Freundlich equations. The Langmuir adsorption capacity, Qmax was found to be 627.1 mg g^{-1}. The Freunlich equation yielded the best fit to the experimental data in comparison to the other isotherm equations. It was found that the adsorption of BB9 increases by increasing the temperature from 293 to 323 K and the process is endothermic in nature. The removal of BB9 by NP-WS followed pseudo-second-order reaction kinetics based on Lagergren equations that showed chemisorption may be the rate-controlling step in the adsorption processes. Obtained results showed complexation and ion exchange appeared to be the principle mechanism for BB9 adsorption.

Keywords: Nanoparticles; Fe_3O_4; Basic Blue 9; Isotherm; Kinetic mechanism

1. Introduction

Many industries, especially textile and food industries often use dyes and pigments to color their products. As a result, textile and food industries often discharge large amounts of colored effluents due to unfixed dyes on fibers or food during coloring and washing steps [1]. The release of these colored wastewaters poses a major problem for the industry as well as a threat to the environment. Color is the first contaminant to be recognized in water and has to be removed from wastewater before discharging in water bodies [2]. The development of an efficient, green, and low-cost method for removal of hazardous organic dye compounds is essential for the environmental protection. Various techniques for removing dyes from effluents have been developed, including electrochemical treatment [3,4], sonochemical treatment [5], photocatalytic oxidation [6,7] and adsorption [8,9], etc. Among them, adsorption is considered as an effective, efficient, and economic method for water purification [10,11]. Since the performance of an adsorptive separation is directly dependent on the quality and cost effectiveness of the adsorbent, the last decade has seen

*Corresponding author.

a continuous improvement in the development of effective noble adsorbents in the form of activated carbon [12], zeolites [13], clay minerals [14], chitosan [15], lignocelluloses [16], natural inorganic minerals [17], functionalized polymers [18], etc. However, most of these adsorbents are either not effective (due to diffusion limitation or the lack of enough active surface sites) or have shown problems like high cost, difficulties of separation from wastewater, or generation of secondary wastes. Considering such drawbacks, recently nano-adsorbents viz. nano-alumina [19], functionalized carbon nanotubes [20], and hydroxyapatite nanoparticles [21] have demonstrated high adsorption efficiency for pollutants removal. One such advanced class of adsorbent–magnetic nanoadsorbent with the help of an external magnetic field has been further successful in circumventing the solid–liquid separation problem usually encountered with nanoparticles. Such novel adsorbent combining nanotechnology and magnetic separation technique has not only demonstrated high adsorption efficiency due to its large surface to volume ratio, but have also shown additional benefits like ease of synthesis, easy recovery, and manipulation via subsequent coating and functionalization, absence of secondary pollutants, cost-effectiveness, and environmental friendliness.

Recently, magnetic separation has been applied in many areas to remove, isolate, and/or concentrate the desired components from a sample solution. Nano-sized magnetic iron oxide particles have been studied extensively as a new adsorbent with large surface area and small diffusion resistance [22] for the separation and removal of chemical species such as metals [23–29], dyes [30–32], and gases [33]. At present, many methods, such as co-precipitation, microemulsion, thermal decomposition, and hydrothermal synthesis, have been applied and reviewed for the production of Fe_3O_4 nanoparticles (NPs) [34,35]. Among these methods, co-precipitation is a facile and convenient method that synthesizes iron oxides from aqueous Fe^{2+}/Fe^{3+} salt solutions in the presence of a base with a high yield and a relatively narrow size distribution [36,37].

Cheaper and effective adsorbents can be formed from abundant natural materials or certain waste materials (or products) from industrial and agricultural activities. In general, an adsorbent which requires little processing or is abundant in nature or is a by-product or waste material from another industry is called a "low-cost" adsorbent [38,39]. In recent years, a vast number of publications have been dedicated to the removal of dye from wastewater by using adsorption techniques with different low-cost materials, such as straw-based adsorbents [40–43].

As an agricultural waste, wheat straw has a high yield every year. However, most of the wheat straw (WS) has been burnt for cooking or heating, or been left directly to decompose. These treatments will not only waste natural resources, but also cause environmental pollution. Therefore, it is necessary to make the best use of wheat straw. Huang et al. have made a comprehensive study for the component, structure, and morphology of wheat straw [44,45]. WS has a vascular bundle structure, which will provide additional surface for chemical modification. It also has complicated components including lignin, hemicellulose, cellulose, pectin, protein, and fatty acid.

The WS is abundant in hydroxyl groups. The hydroxyl groups of wheat straw can provide chemical reaction sites and adsorb iron ions to grow Fe_3O_4 crystal.

In this work, a novel magnetic nanoadsorbent was developed by the surface modification of NPs with WS with the aim of exploring its feasibility as adsorbent for the adsorption of Basic Blue 9 (BB9) taken as a model toxic dye. The objectives of this study are: (1) synthesis of NP-WS by co-precipitation method and their characterization with respect to FE-SEM, X-ray diffraction (XRD), pH_{pzc}, Fourier transform infrared spectroscopy (FTIR), and nitrogen physisorption, (2) comparative batch adsorption study of the NP-WS for BB9 with respect to various environmental parameters, (3) comparative isotherm and kinetic studies, and lastly (4) to presume the underlying mechanism of BB9 binding.

2. Experimental

2.1. Materials

The WS used in this study was obtained from a local wheat field of Ardebil in Iran. The raw material was cleaned and dried at 105°C for 24 h. The dried WS was then ground and sieved into a size range of 100–500 μm. Finally, the resulting product was stored in an air-tight container for further use. The chemical composition of WS was determined as follows: 43.1% cellulose Kurshchner, 19.31% lignin, 29.02% hemicellulose, 6.8% ash, and 1.64% ethanol/dichloromethane extractable, on an oven-dry weight basis (moisture content 7.8%).

The BB9 purchased from Merck (No. 115943), was selected as a representative reactive dye for this study. A stock solution of BB9 was prepared by dissolving 1.0 g of BB9 in 1 L of deionized water, and the concentrations of BB9 used (50–500 mg/L) were obtained by dilution of the stock solution. The pH of the solution

was adjusted to the desired value by adding a small quantity of 0.01 M HCl or 0.01 M NaOH.

2.2. Synthesis of Fe_3O_4/WS and characterization

The chemical precipitation technique has been used to prepare particles with homogeneous composition and narrow size distribution [46]. This technique is probably the most common and efficient method to obtain magnetic particles. A complete precipitation of Fe_3O_4 was achieved under alkaline condition, while maintaining a molar ratio of Fe^{2+} to Fe^{3+}, 1:2, under inert environment. To obtain 2 g of magnetic particles, 2.1 g of $FeSO_4{\cdot}7H_2O$, and 3.1 g of $FeCl_3{\cdot}6H_2O$ were dissolved under inert atmosphere in 80 mL of double distilled water with vigorous stirring. While the solution was heated to 80°C, 10 mL of ammonium hydroxide solution (25%) was added. To ensure complete growth of the nanoparticle crystals, the solution was then added to 10 g of WS and reaction was carried out for 30 min at 80°C under constant stirring. The resulting suspension was cooled down to room temperature and then repeatedly washed with double distilled water to remove unreacted chemicals. Magnetic nanoparticles Fe_3O_4-wheat straw (NP-WS) adsorbent were tested with magnetic rod as shown in Fig. 1, and it is clearly observed that all the iron oxide were attracted to the magnetic rod, because of the magnetic behavior of the iron. The reactions that occur in the production of magnetic nanoparticles (Fe_3O_4-wheat straw) are shown in the following equations:

$$FeSO_4 \cdot 7H_2O + 2FeCl_3 \cdot 6H_2O + 8NH_4OH \rightarrow Fe_3O_4 + 6NH_4Cl + (NH_4)_2SO_4 + 17H_2O \quad (1)$$

$$Fe_3O_4 + WS + 17H_2O \rightarrow \text{NP-WS} \quad (2)$$

The surface structure and morphology of WS, NP-WS before and after BB9 adsorption were characterized using a field emission scanning electron microscopy (Hitachi, S4160, Cold Field Emission) at a 20 kV acceleration voltage. Prior to analysis, the samples were coated with a thin layer of gold. The XRD pattern of NP-WS were obtained by a diffractometer (D8-Advanced, Bruker AXS) with Cu Kα radiation ($\lambda = 1.5406$ nm) in steps of 0.03° (2θ) min^{-1} from $2\theta = 5$ to 70°. The type of binding groups present on the adsorbent were identified by FTIR (Bruker Co. TENSOR 27, Germany) analysis in the region of 400–4,000 cm^{-1} via the KBr pressed disc method. Specific surface area based on nitrogen physisorption was measured by Sibata surface area apparatus 1100. The samples were degassed at 100°C for 2 h prior to the sorption measurement.

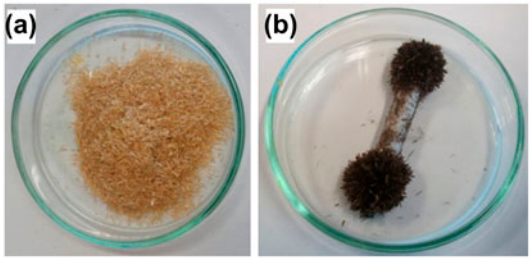

Fig. 1. Photograph of (a) WS and (b) NP-WS attracted by a magnet.

2.3. Studies on point of zero charge (pHpzc)

In pH_{pzc} determination, 0.01 M NaCl was prepared and its pH was adjusted in the range of 2–11 by adding 0.01 M NaOH or HCl. Then, 50 mL of 0.01 M NaCl each was put in conical flask and then 0.1 g of the WS or NP-WS were added to these solutions. These flasks were kept for 72 h and final pH of the solution was measured using pH meter. Graphs were then plotted for pH_{final} vs. $pH_{initial}$.

2.4. Equilibrium and kinetic studies

Equilibrium studies were carried out by contacting fixed amount of NP-WS (0.1 g) with 100 mL of BB9 solution with different initial concentrations (50, 100, 200, 300, 400, and 500 mg/L) in 250 mL stopper Erlenmeyer flasks at a temperature of 30 ± 2°C and pH of 7. The procedure was repeated for temperatures 40 and 50 ± 2°C. BB9 concentrations were determined by spectrometry at the wavelength of maximum absorbance, 664 nm using a double beam UV–vis spectrophotometer (Shimadzu, Model UV 2100, Japan). In kinetics studies, the samples were taken at preset time intervals, and the concentrations of BB9 were measured. Desorption experiments were conducted by shaking 100 mg of adsorbent containing adsorbed BB9 with 100 mL of distilled–deionized water at 298 K and pH 7.0.

2.5. Isotherm modeling

The nonlinear forms of the Langmuir, Freundlich, Temkin, Sips, and Redlich–Peterson isotherm models were used to analyze the equilibrium isotherm data [47]. The fitness of these models was evaluated by the nonlinear coefficients of determination (R^2). The Matlab (version 8.0.0.783) software package was used for computing.

The Langmuir adsorption isotherm assumes that adsorption takes place at specific homogeneous sites within the adsorbent and has found successful application for many processes of monolayer adsorption. The Langmuir isotherm can be written in the following form:

$$Q_e = (Q_{max} k_L C_e)/(1 + K_L C_e) \quad (3)$$

where Q_e is the adsorbed amount of the dye, C_e is the equilibrium concentration of the dye in solution, Q_{max} is the monolayer adsorption capacity and K_L is the Langmuir adsorption constant. The Freundlich isotherm is an empirical equation which assumes that the adsorption occurs on heterogeneous surfaces. The Freundlich equation can be expressed as:

$$Q_e = K_F C_e^{1/n} \quad (4)$$

where K_F and $1/n$ are fitting constants which can be regarded roughly, the capacity and strength of adsorption, respectively. The Sips model is an additional empirical model which has the features of both the Langmuir and Freundlich isotherm models. As a combination of the Langmuir and Freundlich isotherm models, the Sips model contains three parameters, Q_{max}, K_s, and $1/n$, which can be evaluated by fitting the experimental data. The Sips adsorption isotherm model can be written as follows:

$$q_e = (Q_{max} K_S C_e^{1/n})/(1 + K_S C_e^{1/n}) \quad (5)$$

Similar to the Sips isotherm, Redlich and Peterson proposed an isotherm compromising the features of the Langmuir and the Freundlich isotherms:

$$q_e = K_{rp} C_e/(1 + \alpha_{rp} C_e^{\beta}) \quad (6)$$

where K_{rp} and α_{rp} are the Redlich–Peterson constants, and β is basically in the range of zero to one. If β is equal to 1, the equation reduces to the Langmuir isotherm equation, while in case where the value of the term $\alpha_{rp} C_e^{\beta}$ is much bigger than one, the Redlich–Peterson isotherm equation can be approximated by a Freundlich-type equation.

Temkin isotherm was first developed by Temkin and Pyzhevand and it is based on the assumption that the heat of adsorption would decrease linearly with the increase in coverage of adsorbent:

$$q_e = RTln(a_t C_e)/b_t \quad (7)$$

where R is the gas constant, T is the absolute temperature in Kelvin, b_t is the constant related to the heat of adsorption, and a_t is the Temkin isotherm constant. Temkin isotherm equation has been applied to describe the adsorption on heterogeneous surface.

2.6. Kinetic models

The Lagergren rate equation [48] is one of the most widely used adsorption rate equations for the adsorption of solute from a liquid solution. The pseudo-first-order kinetic model of Lagergren may be represented by:

$$dq/q_e - q = k_1 dt \quad (8)$$

Integrating this equation for the boundary conditions $t = 0$ to $t = t$ and $q = 0$ to $q = q_t$, gives:

$$\ln(q_e - q_t) = \ln q_e - k_1 t \quad (9)$$

where q_e and q_t are the amounts of adsorbate (mg/g) at equilibrium and at time t (min), respectively, and k_1 is the rate constant of pseudo-first-order adsorption (min^{-1}). The validity of the model can be checked by a linearized plot of $\ln(q_e - q_t)$ versus t. Also, the rate constant of pseudo-first-order adsorption is determined from the slope of the plot.

The pseudo-second-order equation based on adsorption equilibrium capacity can be expressed as:

$$dq/(q_e - q_t)^2 = k_2 dt \quad (10)$$

Taking into account, the boundary conditions $t = 0$ to $t = t$ and $q = 0$ to $q = q_t$, the integrated linear form of the above equation can be rearranged to follow an equation:

$$1/(q_e - q_t) - 1/q_e = k_2 t \quad (11)$$

Rearranging the variables gives the following equation:

$$t/q_t = 1/k_2 q_e^2 + t/q_e \quad (12)$$

where the theoretical equilibrium adsorption capacity (q_e) and the second-order constants k_2 ($g\ mg^{-1}\ min^{-1}$) can be determined experimentally from the slope and intercept of plot t/q vs. t.

3. Results and discussion

3.1. XRD, FE-SEM analysis, and nitrogen physisorption

The powder XRD patterns of WS and NP-WS are shown in Fig. 2. WS consists of mainly crystalline cellulose, and noncrystalline hemicellulose and lignin [44]. The diffraction peaks at $2\theta^\circ = 16.1$ and 22.4° for cellulose I crystalline form, which is assigned to most natural cellulose [44]. The main crystal planes in a pure Fe_3O_4 crystals ($2\theta^\circ = 19.375$, 30.535, 35.695, 43.315, 57.805, and 62.935), marked by their indices ((1 1 1), (2 2 0), (3 1 1), (4 0 0), (5 1 1), and (4 4 0)), were reported. The diffraction peaks of Fe_3O_4 match well with the inverse cubic spinel structure (JCPDS 19-0629). The XRD pattern of NP-WS confirms that the nano Fe_3O_4 was loaded on WS which contributed to the super-paramagnetic of NP-WS. Comparing with XRD pattern of pure Fe_3O_4 (not shown), the peak intensity of NP-WS decreases and the full width of the peak increases, which indicates the low crystallinity and small crystallite size. It can be predominantly attributed to the existence of the WS which affects the crystal size and crystallinity. The average particle size of NPs on WS can be calculated using Scherrer's equation:

$$n = K\lambda/\beta_{1/2}\cos\theta \tag{13}$$

where K is the Scherrer's constant with value from 0.9 to 1 (shape factor), where λ is the X-ray wavelength (1.5406 Å), $\beta_{1/2}$ is the width of the XRD peak at half height, and θ is the Bragg angle. From the Scherrer's equation, the average crystallite size of NPs for WS is found to be less than 30 nm, which was also in line with the observation of the FE-SEM results.

FE-SEM images for the WS, NP-WS before and after BB9 adsorption are shown in Fig. 3(a–c). The WS materials have insoluble cell walls with fibrous content and are largely made up of cellulose-based structural proteins. A high response surface of the functional groups is also present. Fig. 3(b) shows the WS is completely covered with iron oxide, and all the iron oxide particles are aggregated to form a spherical and cage-like structure. The presence of

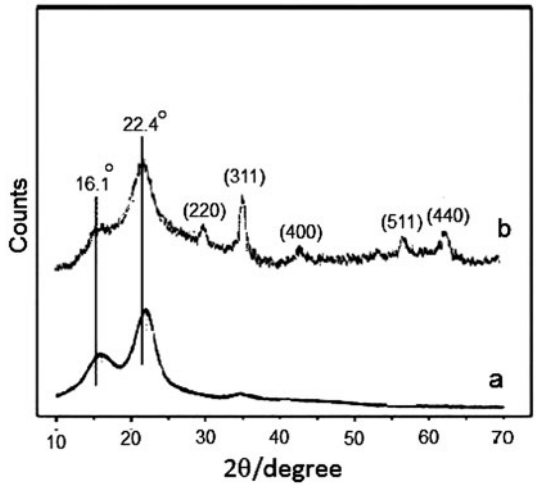

Fig. 2. XRD patterns of (a) WS and b) NP-WS.

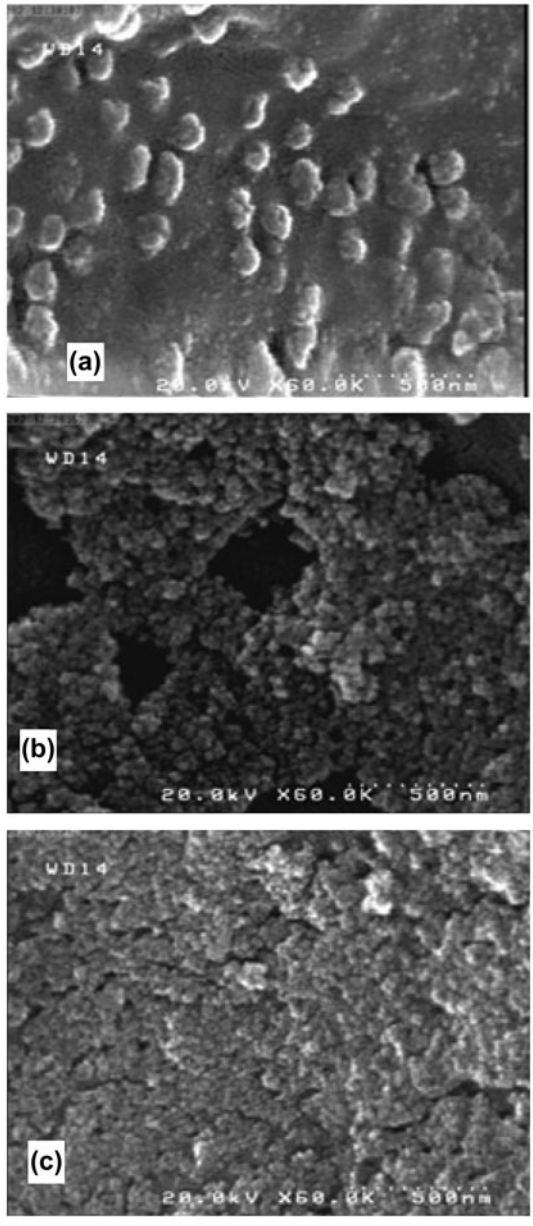

Fig. 3. FE-SEM images of (a) WS, b) NP-WS and (c) NP-WS after BB9 adsorption.

nano Fe_3O_4 on the NP-WS surface possesses a favorable superparamagnetism and is consistent with the results from Fig. 1 that was attracted by magnetic rod [49]. Fig. 3(c) shows the FE-SEM image, after BB9 adsorption onto NP-WS. Compared to Fig. 3(b), more particles are present on the surface of the NP-WS. These particles are the BB9 dye molecules as well as the iron oxide particles. The iron oxide particles exhibit magnetic behavior, creating more negative charges [50]. The positively charge BB9 will be electrostatically attracted to the adsorbent. This is depicted by more particles being adsorbed as shown in Fig. 3(c).

The specific surface area of WS and NP-WS before and after BB9 adsorption based on nitrogen physisorption was determined by Brunauer–Emmett–Teller (BET) theory. It was found that the surface area of WS and NP-WS before and after BB9 adsorption were 15.8, 36.5, and 74.6 $m^2 g^{-1}$, respectively.

3.2. FTIR analysis

The FTIR spectra of NP-WS before and after BB9 adsorption are shown in Fig. 4. The peak at 668 cm^{-1} observed in Fig. 4(a) is related to the Fe–O group and the peak around 3,447 cm^{-1} in curve was assigned to the –OH group on the surface of the magnetite [20]. These two significant bands in the spectrum indicate the possible involvement of those functional groups on the surface of NP-WS process. Thus, it seems that this type of functional group is likely to participate in BB9 binding. In comparison with WS (spectrum not shown), NP-WS showed decrease in the intensity of the adsorption peaks. This result indicated that Fe_3O_4 NPs could be successfully coated on the surface of WS [51]. Fig. 4(b) shows the FTIR spectrum after adsorption of BB9 onto NP-WS. When comparing the two spectra of Fig. 4(a) and (b), Fig. 4(b) shows that the hydroxyl groups are present in the range of peak at 3,429 cm^{-1}. This peak has shifted and changes the region of the peaks (indicated by asterisks), because the hydroxyl groups are likely to participate in the BB9 adsorption. A well-known mechanism involved in the adsorbate and adsorbent interaction is governed by ion exchange process and followed by the adsorption process. In the adsorption process, H^+ ions leaving functional groups of the adsorbent bound with BB9 at the adsorbent surface due to electrostatic attraction. We will discuss about adsorption mechanism in next section.

3.3. Determination of point of zero charge (pH_{pzc}) and underlying mechanism

The point of zero charge (pH_{pzc}) is an important factor that determines the linear range of pH sensitivity and then indicates the type of surface active centers and the adsorption ability of the surface [52]. Many researchers studied the point of zero charge of adsorbents that prepared from agricultural solid wastes in order to better understand of adsorption mechanism. Cationic dye adsorption is favored at pH > pH_{pzc}, due to the presence of functional groups such as OH^-, COO^- groups. Anionic dye adsorption is favored at pH < pH_{pzc} where the surface becomes positively charged [53,54]. The graph of pH_{intial} vs. pH_{final} was plotted as shown in Fig. 5. The intersections of

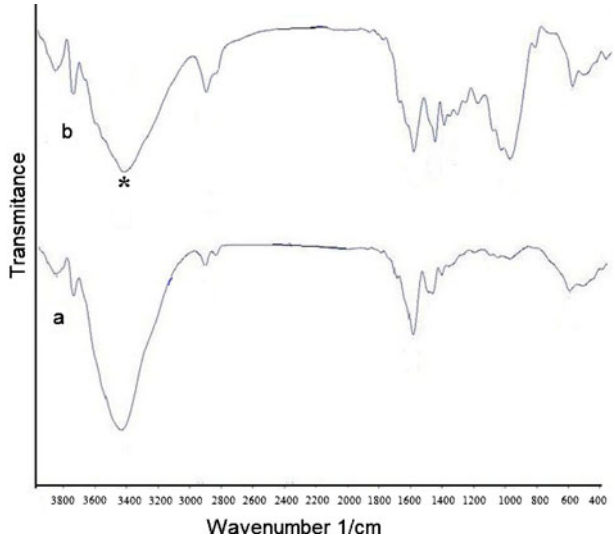

Fig. 4. FTIR spectra of NP-WS (a) before and (b) after BB9 adsorption.

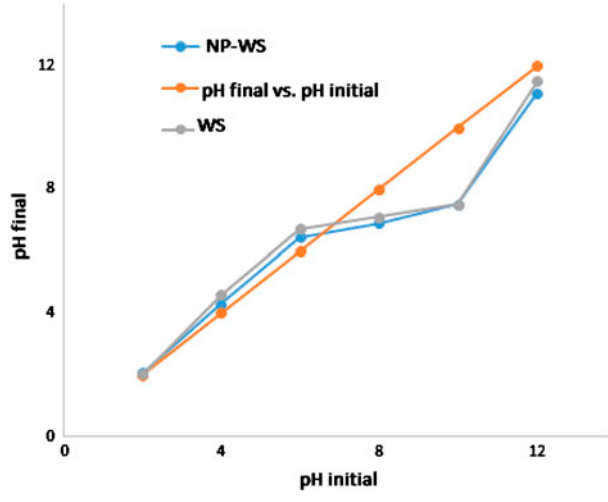

Fig. 5. Plot determination for point of zero charge of NP-WS.

the curves with the straight line are known as the end points of the pH_{pzc}, and this value is 6.8 for NP-WS. The surface of NP-WS was positively charged at pH < 6.8, not only the weak physical forces such as hydrogen bonding, van der Waals interactions but also the chemisorption might be involved in the adsorption process [2]. At pH > 6.8, the surface of the adsorbent became negatively charged; the increased adsorption capacity was likely assigned to the electrostatic forces and the improvement of chemical action.

According to the acid–base equilibrium of BB9 or MB represented by $MBH^{2+} \leftrightarrow MB^{+} + H^{+}$, and to its very low pK_a value (less than 1) the removal of BB9 was due mainly to solubilization of unprotonated form of the dye MB^{+} [55]. At low pH values, the poor adsorption of BB9 could be due to competition with the H^{+} ions for binding sites on NP-WS. Moreover, many protons will be available to protonate the NP-WS surface in the condition; thereby, the electrostatic repulsion between positively charged MB^{+} and positively charged adsorption sites causes the decrease in the dye adsorption. As the pH increased, the NP-WS surface was more negatively charged and the functional groups (such as carboxyl ($pK_a = 4.02$), amino ($pK_a = 9.39$), and hydroxyl ($pK_a = 8.36$) groups) would be more deprotonated [56], thus attraction of MB^{+} was enhanced. The observed trend can be explained by the effect of the surface charge of adsorbent and pH_{pzc} as reported by Gupta and Nyaka [57]. The multi hydroxyl groups on NP-WS as revealed by FTIR spectra play a dominant role in the BB9 adsorption. Depending upon the solution pH, the adsorbent surface undergoes protonation or deprotonation [58].

The protonation/deprotonation reaction for NP-WS undergoes as follows:

$$\text{–Fe–O–(C=O)–(OH)}_{\mathbf{n}} + H^{+} \rightarrow \text{–Fe–O–(C=O)–(OH)}_2)_{n}^{+} \quad (14)$$

At pH < pH_{pzc} (pH_{pzc} of NP-WS is 6.8) –Fe–O–(C=O)–$(OH)_n^{+}$ are the dominant species for NP-WS. These species having high positive charge density make the BB9 dye cation adsorption unfavorable due to electrostatic repulsion. Also, stiff competition between H^{+} and BB9 dye cation for the active sites will decrease BB9 adsorption [27]. But, at pH > pH_{pzc}, –Fe–O–(C=O)–$(OH)_n$ are the dominant species in NP-WS. Such deprotonated species undergo electrostatic attraction for BB9 dye cation that results in the formation of BB9–Fe_3O_4 magnetic composite complexes. This causes enhanced adsorption. Complexation and ion exchange appear to be the principle mechanism of the adsorption as revealed by the following equation:

$$\text{–Fe–O–(C=O)–(OH)}_{\mathbf{n}} + \text{BB9} \rightarrow \text{–Fe–O–(C=O)–(O–BB9)}_{n}^{+} + nH^{+} \quad (15)$$

We studied the pH effect on adsorption of BB9 within pH range 2.0–12.0 (results not shown). The uptake of BB9 increased with the increase in the solution pH and the maximum uptake of BB9 was observed at pH 7.0. At low pH values, the poor adsorption of BB9 could be due to competition with the H^{+} ions for binding sites on NP-WS. Moreover, many protons will be available to protonate the NP-WS surface in the condition; thereby, the electrostatic repulsion between positively charged BB9 ions and positively charged adsorption sites causes the decrease in the dye adsorption. As the pH increased, the NP-WS surface was more negatively charged and the functional groups (such as carboxyl, amino, and hydroxyl groups) would be more deprotonated, thus attraction of BB9 ions was enhanced. These data are in good agreement with the determination of point of zero charge.

3.4. Isotherm modeling

Analysis of the isotherm data is important to develop equations that correctly represent the results and could be used for design purposes. Fig. 6 and Table 1 show the fitting parameters for the measured isotherm data for BB9 adsorption onto NP-WS on the nonlinear forms of Langmuir, Freundlich, Temkin, Redlich–Peterson, and Sips models. The values of nonlinear correlation coefficients (R^2) for the Langmuir, Sips, Freundlich, and Rudlich–Peterson isotherm models indicate good fit with the four models. The applicability of Langmuir, Sips and Rudlich–Peterson isotherms showed that there were effectively monolayer sorption and a homogeneous distribution of active sites on the surface of adsorbent. In all the temperatures, the Temkin isotherm represented the poorest fit of experimental data in comparison with other isotherm equations. The Freunlich equation yielded the best fit to the experimental data in comparison with other isotherm equations in this study. The value of exponent $1/n$ for the Sips model is close to unity indicating that adsorptions are rather homogeneous. The maximum BB9 adsorption capacity ($mg\,g^{-1}$) belongs to NP-WS which has been shown in Table 1. The monolayer capacity (Qmax) is 627.1 $mg\,g^{-1}$ as calculated from Langmuir model at 323 K. The adsorption capacities of magnetic nanoparticle loaded on wheat straw (NP-WS), used in the present study, are significant. The manufacture of this adsorbent could be upscaled and produced in small-scale industries.

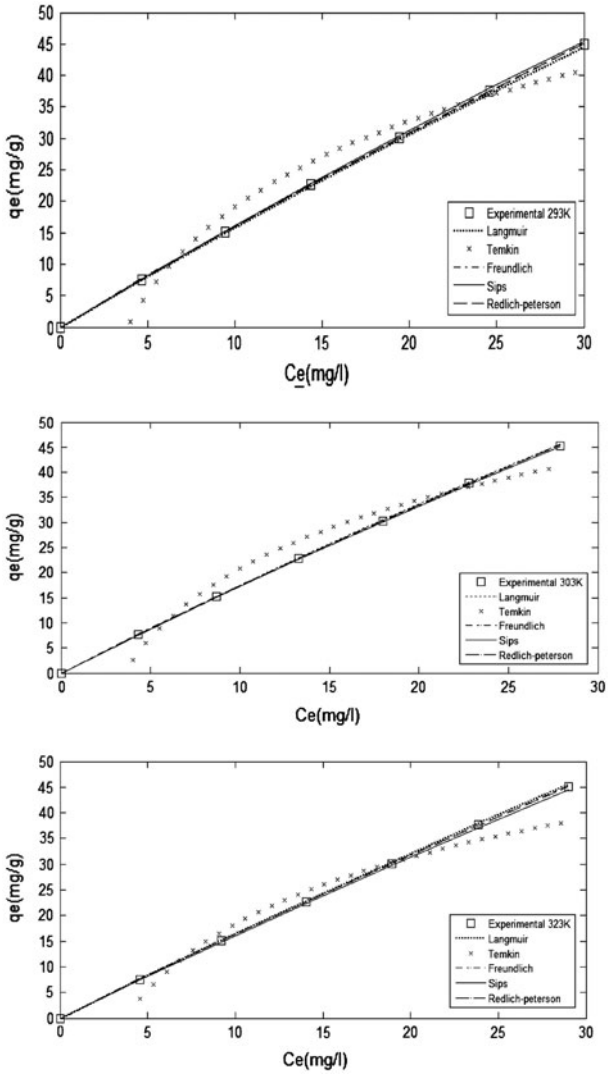

Fig. 6. Isotherm plots for BB9 adsorption onto NP-WS at different temperatures.

The Freundlich model assumes that the uptake of BB9 occurs on a heterogeneous adsorbent surface. The magnitude of the Freundlich constant n gives a measure of favorability of adsorption. Values of $n > 1$ represent a favorable adsorption process [21]. For the present study, the value of n also presents the same trend at all the temperatures indicating favorable nature of adsorption of BB9 by NP-WS.

3.5. Adsorption kinetics studies

The dynamics of the adsorption can be studied by the kinetics of adsorption in terms of the order of the rate constant [59]. The adsorption rate is an important factor for a better choice of material to be used as an adsorbent, where the adsorbent should have a large adsorption capacity and a fast adsorption rate. Most of the adsorption studies used pseudo-first-order and pseudo-second-order models to study the adsorption kinetics. For the pseudo-first-order model, the adsorption rate was expected to be proportional to the first power of concentration, where the adsorption was characterized by diffusion through a boundary. The pseudo-first-order model sometimes does not fit well for the whole range of contact time when it failed theoretically to predict the amount of dye adsorbed and thus deviated from the theory. In that case, the pseudo-second-order equation used was based on the sorption capacity of the solid phase, where the pseudo-second-order model assumes that chemisorption may be the rate-controlling step in the adsorption processes [60,61].

The transient behavior of the BB9 adsorption process was analyzed by using the pseudo-first-order and pseudo-second-order kinetic models. Plotting ln $(q_e - q_t)$ against t permits calculation of k_1 (Fig. 7(a)). The rate constants, k_1, evaluated from these plots with the correlation coefficients obtained are listed in Table 2. Plotting t/q against t (Fig. 7(b)), gives a straight line where k_2 can be calculated. Usually the best-fit model can be selected based on the linear regression correlation coefficient R^2 values. Generally the kinetic adsorption is better represented by pseudo-second-order model for

Table 1
Isotherm parameters for BB9 adsorption onto NP-WS

Temperature (K)	293	303	323
Langmuir			
Q_{max} (mg/g)	494.4	544.6	627.1
K (L/mg)	0.0033	0.0040	0.0057
R^2	0.9961	0.9949	0.9966
Freundlich			
$1/n$	0.9444	0.9397	0.9557
k_F (mg/g) (L/mg)$^{1/n}$	1.8190	2.001	1.8120
R^2	0.9999	0.9998	0.9999
Temkin			
B	123.086	126.679	134.379
k_T (L/mg)	0.2620	0.2841	0.2664
R^2	0.9429	0.9436	0.9414
Sips			
Q_{max} (mg/g)	445.8	491.3	663
b ((mg^{-1})$^{-1/n}$)	0.00366	0.00453	0.00554
$1/n$	1.007	1.011	0.9974
R^2	09,961	0.9949	0.9966
Redlich–Peterson			
a (L kg^{-1})	1.638	1.784	1.684
B (kg mg^{-1})	0.0018	0.0015	0.0036
n	1.152	1.244	0.9294
R^2	0.9959	0.9960	0.9966

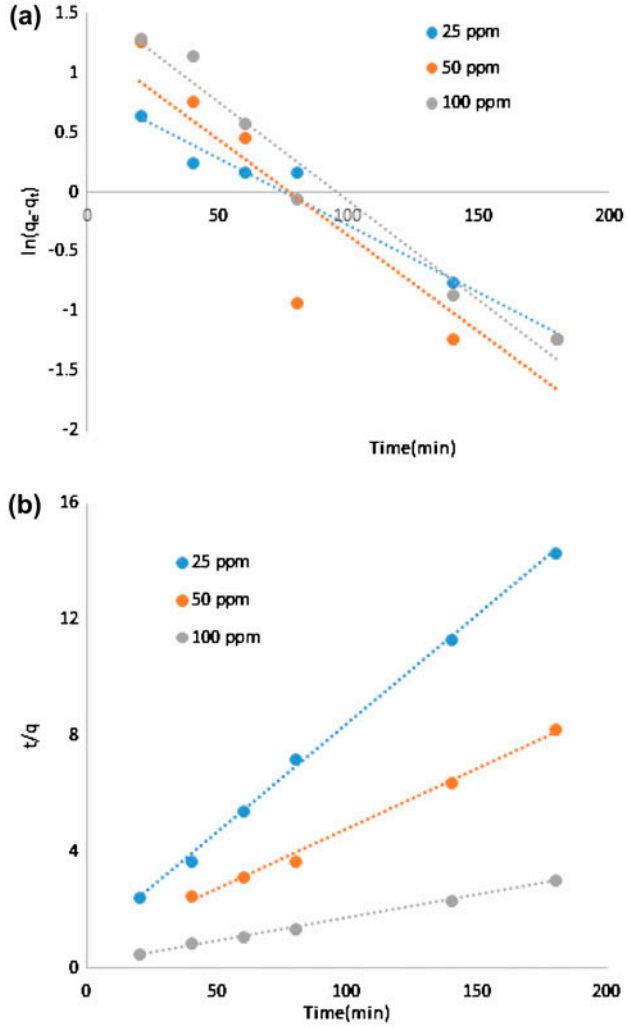

Fig. 7. Kinetic models for adsorption of BB9 onto NP-WS. (a) Pseudo-first-order and (b) pseudo-second-order rate equations.

Table 2
Kinetic parameters for the adsorption of BB9 onto NP-WS based on Lagergren rate equation

C_0 (mg/L)	25	50	100
Pseudo-first-order equation			
k_1 (min^{-1})	0.0113	0.0161	0.0166
q_e (mg g^{-1})	2.3554	3.4963	4.8939
R^2	0.9692	0.8063	0.9648
Pseudo-second-order equation			
k_2 (g mg^{-1} min^{-1})	0.0059	0.002710	0.001353
q_e (mg g^{-1})	13.42	24.04	64.10
R^2	0.9985	0.9943	0.9974

anionic and cationic dye adsorption. Lakshmi et al. [62] evaluated the adsorption of Indigo carmine dye by rice husk ash. They found that the values of the pseudo-first-order rate constant increases from 0.0087 to 0.0122 min^{-1} with an increasing initial dye concentration from 50 to 500 mg/L, which indicates that the adsorption rate increases with an increase in initial dye concentration while the R^2 values were closer to unity for the pseudo-second-order model than that for the pseudo-first-order model. Ponnusami et al. [63] studied the use of guava leaf powder for adsorption of methylene blue. They found that the values of R^2 of the pseudo-first-order model were between 0.70 and 0.85, while the values of R^2 for the second-order model were 0.999, indicating the conformity of second-order model.

The R^2 listed (in Table 2) for the pseudo-first-order kinetic model was between 0.80631 and 0.0.9692. The R^2 values for pseudo-second-order model were >0.9943, which is higher than the R^2 values obtained for the pseudo-first-order model. Therefore, the adsorption kinetics could well be satisfactorily more favorably described by pseudo-second-order kinetic model for BB9 adsorption onto NP-WS.

3.6. BB9 desorption studies

The tests of BB9 desorption were conducted with three initial BB9 concentrations (50, 100, and 200 mg/L). The BB9 desorbability can be defined as the ratio of the desorbed BB9 over the total adsorbed BB9 by the adsorbent. Therefore, the desorbability of BB9 can be used to indicate the degree of BB9 desorption from the adsorptive materials. The obtained data show that the desorbability of BB9 is about 10–14%, and the amount of the desorbed BB9 is slightly increased with the increase in adsorbed BB9. These results indicate that the BB9 adsorption on the NP-WS is not completely reversible and the bonding between the NP-WS and adsorbed BB9 is likely strong. It is relatively difficult for the adsorbed BB9 to be desorbed from the NP-WS.

3.7. Comparison with other bioadsorbents

A comparison of the maximum adsorption capacity (Q_{max} value) of NP-WS with those of other low-cost adsorbents in the literatures is shown in Table 3. The NP-WS shows the comparable adsorption capacity for BB9 with respect to other low-cost adsorbents. However, the adsorption capacity was higher than those of other adsorbents. Therefore, NP-WS was suitable and promising for BB9 removal from aqueous solutions since it has a relatively high adsorption capacity and was easily recovered from treated effluents by applying a magnet.

Table 3
Comparison of the Q_{max} based on Langmuir isotherm of BB9 on various adsorbents

Adsorbent	Q_{max} (mg/g)	Reference
NP-WS	627.1	This work
Wheat straw	57.2	[42]
Carboxymethylation wheat straw	266.7	[42]
NaOH-modified rejected tea	242.11	[64]
Fe_3O_4–maize cob	70.29	[65]
Citric acid treated wheat straw	450	[66]
Modified rice straw	208.33	[67]

4. Conclusion

The efficiency of nanoparticle Fe_3O_4 loaded onto wheat straw in adsorption of BB9 dye from aqueous solution has been investigated. Results indicate that adsorption is positively dependent on pH and temperature. The adsorption isotherm data showed the best fitting to Freundlich isotherm. The adsorption capacity was found to be 627.1 mg g^{-1}. The kinetics of adsorption followed pseudo-second-order kinetics. The adsorption efficiency increases with the increase in temperature and hence adsorption process is endothermic in nature. The developed NP-WS not only has demonstrated higher adsorption efficiency and fast kinetics but also have shown additional benefits like ease of synthesis, easy recovery, absence of secondary pollutants, cost-effectiveness, and environmental-friendliness. It can be concluded to be a promising advanced adsorbent in environmental pollution cleanup.

Acknowledgment

The authors wish to acknowledge the financial support of the University of Tehran.

References

[1] S.C.R. Santos, R.A.R. Boaventura, Adsorption modelling of textile dyes by sepiolite, Appl. Clay Sci. 42 (2008) 137–145.
[2] M.S. Chiou, P.Y. Ho, H.Y. Li, Adsorption of anionic dyes in acid solutions using chemically cross-linked chitosan beads, Dyes Pigm. 60 (2004) 69–84.
[3] B. Korbahti, Response surface optimization of electrochemical treatment of textile dye wastewater, J. Hazard. Mater. 145 (2007) 277–286.
[4] Z.M. Shen, D. Wu, J. Yang, T. Yuan, W.H. Wang, J.P. Jia, Methods to improve electrochemical treatment effect of dye wastewater, J. Hazard. Mater. B131 (2006) 90–97.
[5] S. Wang, Z.H. Zhu, Sonochemical treatment of fly ash for dye removal from wastewater, J. Hazard. Mater. B126 (2005) 91–95.
[6] H.Y. Zhu, R. Jiang, Y.J. Guan, Y.Q. Fu, L. Xiao, G.M. Zeng, Effect of key operational factors on decolourization of methyl orange during H_2O_2 assisted nanosized CdS/TiO_2/polymer composite thin films under simulated solar light irradiation, Sep. Purif. Technol. 74 (2010) 187–194.
[7] R. Jiang, H.Y. Zhu, Y.J. Guan, Y.Q. Fu, L. Xiao, Q.Q. Yuan, S.T. Jiang, Effective decolorization of azo dye utilizing SnO_2/CuO/polymer films under simulated solar light irradiation, Chem. Eng. Technol. 34(2) (2011) 17–185.
[8] L. Lian, L. Guo, C. Guo, Adsorption of Congo red from aqueous solutions onto Ca-bentonite, J. Hazard. Mater. 161 (2009) 126–131.
[9] E. Bulut, M. Ozacar, I.A. Sengil, Equilibrium and kinetic data and process design for adsorption of congo Red onto bentonite, J. Hazard. Mater. 154 (2008) 613–622.
[10] V.K. Gupta, P.J.M. Carrott, M.M.L. Ribeiro Carrott, Suhas, Low-cost adsorbents: Growing approach to wastewater treatment—A review, Crit. Rev. Environ. Sci. Technol. 39 (2009) 783–842.
[11] I. Ali, V.K. Gupta, Advances in water treatment by adsorption technology, Nat. Protoc. 1 (2007) 2661–2667.
[12] X. Huang, N.Y. Gao, Q.L. Zhang, Thermodynamics and kinetics of cadmium adsorption onto oxidized granular activated carbon, J. Environ. Sci. 19 (2007) 1287–1292.
[13] M.R. Panuccio, A. Sorgonà, M. Rizzo, G. Cacco, Cadmium adsorption on vermiculite, zeolite and pumice: Batch experimental studies, J. Environ. Manage. 90 (2009) 364–374.
[14] J. Hizal, R. Apak, Modeling of cadmium (II) adsorption onkaolinite-based clays in the absence and presence of humic acid, Appl. Clay Sci. 32 (2006) 232–244.
[15] J.T. Bamgbose, S. Adewuyi, O. Bamgbose, A.A. Adetoye, Adsorption kinetics of cadmium and lead by chitosan, Afr. J. Biotechnol. 9 (2010) 2560–2565.
[16] E.W. Shin, K.G. Karthikeyan, M.A. Tshabalala, Adsorption mechanism of cadmium on juniper bark and wood, Bioresour. Technol. 98 (2007) 588–594.
[17] K. Sevgi, Adsorption of Cd(II), Cr(III) and Mn(II) on natural sepiolite, Desalination 244 (2009) 24–30.
[18] G.C. Panda, S.K. Das, A.K. Guha, Biosorption of cadmium and nickel by functionalized husk of *Lathyrus-sativus*, Colloids Surf., B 62 (2008) 173–179.
[19] V. Srivastava, C.H. Weng, V.K. Singh, Y.C. Sharma, Adsorption of nickel ions from aqueous solutions by nano alumina: Kinetic, mass transfer, and equilibrium studies, J. Chem. Eng. Data 56 (2011) 1414–1422.
[20] V.K. Gupta, S. Agarwal, T.A. Saleh, Synthesis and characterization of alumina-coated carbon nanotubes and their application for lead removal, J. Hazard. Mater. 185 (2011) 17–23.
[21] Y. Feng, J.-L. Gong, G.-M. Zeng, Q.-Y. Niu, H.-Y. Zhang, C.-G. Niu, J.-H. Deng, M. Yan, Adsorption of Cd(II) and Zn(II) from aqueous solutions using magnetic hydroxyapatite nanoparticles as adsorbents, Chem. Eng. J. 162 (2010) 487–494.
[22] M.H. Liao, D.H. Chen, Fast and efficient adsorption/desorption of protein by a novel magnetic nano-adsorbent, Biotechnol. Lett. 24 (2002) 1913–1917.

[23] L. Wang, Z. Yang, J. Gao, K. Xu, H. Gu, B. Zhang, X. Zhang, B. Xu, A biocompatible method of decorporation: Bisphosphonate modified magnetite nanoparticles to remove uranyl ions from blood, J. Am. Chem. Soc. 128 (2006) 13358–13359.
[24] J.T. Mayo, C. Yavuz, S. Yean, L. Cong, H. Shipley, W. Yu, J. Falkner, A. Kan, M. Tomson, V.L. Colvin, The effect of nanocrystalline magnetite size on arsenic removal, Sci. Technol. Adv. Mater. 8 (2007) 71–75.
[25] A. Uheida, G. Salazar-Alvarez, E. Björkman, Z. Yu, M. Muhammed, Fe_3O_4 and gamma-Fe_2O_3 nanoparticles for the adsorption of Co^{2+} from aqueous solution, J. Colloid. Interface Sci. 298 (2006) 501–507.
[26] C. Huang, B. Hu, Silica-coated magnetic nano-particles modified with gamma-mercaptopropyltrime-thoxysilane for fast and selective solid phase extraction of trace amounts of Cd, Cu, Hg, and Pb in environmental and biological samples prior to their determination by inductively coupled plasma mass spectrometry, Spectrochim. Acta B 63 (2008) 437–444.
[27] J.E. Macdonald, J.A. Kelly, J.G.C. Veinot, Iron/iron oxide nanoparticle sequestration of catalytic metal impurities from aqueous media and organic reaction products, Langmuir 23 (2007) 9543–9545.
[28] M. Faraji, Y. Yamini, M. Rezaee, Extraction of trace amounts of mercury with sodium dodecyl sulphate-coated magnetite nanoparticles and its determination by flow injection inductively coupled plasma-optical emission spectrometry, Talanta 81 (2010) 831–836.
[29] M. Faraji, Y. Yamini, A. Saleh, M. Rezaee, M. Ghambarian, R. Hassani, A nanoparticle-based solid-phase extraction procedure followed by flow injection inductively coupled plasma-optical emission spectrometry to determine some heavy metal ions in water samples, Anal. Chim. Acta 659 (2010) 172–177.
[30] N. Yang, S. Zhu, D. Zhang, S. Xu, Synthesis and properties of magnetic Fe_3O_4-activated carbon nanocomposite particles for dye removal, Mater. Lett. 62 (2008) 645–647.
[31] Y.C. Chang, D.H. Chen, Adsorption kinetics and thermodynamics of acid dyes on a carboxymethylatedchitosan-conjugated magnetic nano-adsorbent, Macromol. Biosci. 5 (2005) 254–261.
[32] M.H. Liao, K.Y. Wu, D.H. Chen, Fast removal of basic dyes by a novel magnetic nanoadsorbent, Chem. Lett. 6 (2003) 488–489.
[33] P. Li, D.E. Miser, S. Rabiei, R.T. Yadav, M.R. Hajaligol, The removal of carbon monoxide by iron oxide nanoparticles, Appl. Catal., B 43 (2003) 151–162.
[34] M. Faraji, Y. Yamini, M. Rezaee, Magnetic nanoparticles: Synthesis, stabilization, functionalization, characterization, and applications, J. Iran Chem. Soc. 7 (2010) 1–37.
[35] A.-H. Lu, E.L. Salabas, F. Schuth, Magnetic nanoparticles: Synthesis, protection, functionalization, and application, Angew. Chem. Int. Ed. 46 (2007) 1222–1244.
[36] J. Park, K. An, Y. Hwang, J.G. Park, H.J. Noh, J.Y. Kim, J.H. Park, N.M. Hwang, T. Hyeon, Ultra-large-scale syntheses of monodispersenanocrystals, Nat. Mater. 3 (2004) 891–895.
[37] J.H. Jang, H.B. Lim, Characterization and analytical application of surface modified magnetic nanoparticles, Microchem. J. 94 (2010) 148–158.
[38] M. Rafatullah, O. Sulaiman, R. Hashim, A. Ahmad, Adsorption of methylene blue on low-cost adsorbents: A review, J. Hazard. Mater. 177 (2010) 70–80.
[39] V.K. Gupta, Suhas, Application of low-cost adsorbents for dye removal—A review, J. Environ. Manage. 90 (2009) 2313–2342.
[40] W. Zhang, H. Yang, L. Dong, H. Yan, H. Li, Z. Jiang, X. Kan, A. Li, R. Cheng, Efficient removal of both cationic and anionic dyes from aqueous solutions using a novel amphoteric straw-based adsorbent, Carbohydr. Polym. 90 (2012) 887–893.
[41] W. Zhang, H. Li, X. Kan, L. Dong, H. Yan, Z. Jiang, H. Yang, A. Li, R. Cheng, Adsorption of anionic dyes from aqueous solutions using chemically modified straw, Bioresour. Technol. 117 (2012) 40–47.
[42] W. Zhang, H. Yan, H. Li, Z. Jiang, L. Dong, X. Kan, H. Yang, A. Li, R. Cheng, Removal of dyes from aqueous solutions by straw based adsorbents: Batch and column studies, Chem. Eng. J. 168 (2011) 1120–1127.
[43] W. Zhang, L. Dong, H. Yan, H. Li, Z. Jiang, X. Kan, H. Yang, A. Li, R. Cheng, Removal of methylene blue from aqueous solutions by straw based adsorbents in a fixed-bed column, Chem. Eng. J. 173 (2011) 429–436.
[44] R. Liu, H. Yu, Y. Huang, Structure and morphology of cellulose in wheat straw, Cellulose 12 (2005) 25–34.
[45] H. Yu, R. Liu, D. Shen, Y. Jiang, Y. Huang, Study on morphology and orientation of cellulose in the vascular bundle of wheat straw, Polymer 46 (2005) 5689–5694.
[46] S. Laurent, D. Forge, M. Port, A. Roch, C. Robic, L. Vander Elst, R.N. Muller, Magnetic iron oxide nanoparticles: Synthesis, stabilization, vectorization, physicochemical characterizations, and biological applications, Chem. Rev. 108 (2008) 2064–2110.
[47] Y. Liu, Y.J. Liu, Biosorption isotherms, kinetics and thermodynamics, Sep. Purif. Technol. 61 (2008) 229–238.
[48] S. Lagergren, B.K. Svenska, About the theory so-called adsorption of soluble substance, K. Sven Vetenskapsakad. Handl. 24 (1898) 1–39.
[49] S. Bahçeci, B. Unal, A. Baykal, H. Sözeri, E. Karaoglu, B. Esat, Synthesis and characterization of polypropiolate sodium (PPNa)–Fe_3O_4 nanocomposite, J. Alloys Compd. 509 (2011) 8825–8831.
[50] P. Panneerselvam, N. Morad, K.A. Tan, Magnetic nanoparticle (Fe_3O_4) impregnated onto tea waste for the removal of nickel (II) from aqueous solution, J. Hazard. Mater. 186 (2011) 160–168.
[51] Y.P. Chang, C.L. Ren, J.C. Qu, Preparation and characterization of Fe_3O_4/grapheme nanocomposite and investigation of its adsorption performance for aniline and p-chloroaniline, Appl. Surf. Sci. 261 (2012) 504–509.
[52] A.A. Poghossian, Determination of the pH_{pzc} of insulators surface from capacitance–voltage characteristics of MIS and EIS structures, Sens. Actuator, B 44 (1997) 551–553.
[53] L.R. Radovic, I.F. Silva, J.I. Ume, J.A. Menedez, C.A. Leon, A.W. Scaroni, An experimental and theoretical study of the adsorption of aromatics possessing electron-withdrawing and electron-donating functional groups by chemically modified activated carbons, Carbon 35 (1997) 1339–1348.

[54] D. Savova, N. Petrov, M.F. Yardim, E. Ekinci, T. Budinova, M. Razvigorova, V. Minkova, The influence of the texture and surface properties of carbon adsorbents obtained from biomass products on the adsorption of manganese ions from aqueous solution, Carbon 41 (2003) 1897–1903.
[55] N. Zaghbani, A. Hafiane, M. Dhahbi, Separation of methylene blue from aqueous solution by micellar enhanced ultrafiltration, Sep. Purif. Technol. 55 (2007) 117–124.
[56] Y. Tian, C. Ji, M. Zhao, M. Xu, Y. Zhang, R. Wang, Preparation and characterization of baker's yeast modified by nano-Fe_3O_4: Application of biosorption of methyl violet in aqueous solution, Chem. Eng. J. 165 (2010) 474–481.
[57] V.K. Gupta, A. Nayak, Cadmium removal and recovery from aqueous solutions by novel adsorbents prepared from orange peel and Fe_2O_3 nanoparticles, Chem. Eng. J. 180 (2012) 81–90.
[58] S.S. Banerjee, D.H. Chen, Fast removal of copper ions by gum arabic modified magnetic nano-adsorbent, J. Hazard. Mater. 147 (2007) 792–799.
[59] V. Gómez, M.S. Larrechi, M.P. Callao, Kinetic and adsorption study of acid dye removal using activated carbon, Chemosphere 69 (2007) 1151–1158.
[60] G. Crini, P.-M. Badot, Application of chitosan, a natural aminopolysaccharide, for dye removal from aqueous solutions by adsorption processes using batch studies: A review of recent literature, Prog. Polym. Sci. 33 (2008) 399–447.
[61] Z. Aksu, Application of biosorption for the removal of organic pollutants: A review, Process Biochem. 40 (2005) 997–1026.
[62] U.R. Lakshmi, V.C. Srivastava, I.D. Mall, D.H. Lataye, Rice husk ash as an effective adsorbent: Evaluation of adsorptive characteristics for Indigo Carmine dye, J. Environ. Manage. 90 (2009) 710–720.
[63] V. Ponnusami, S. Vikram, S.N. Srivastava, Guava (*Psidium guajava*) leaf powder: Novel adsorbent for removal of methylene blue from aqueous solutions, J. Hazard. Mater. 152 (2008) 276–286.
[64] N. Nasuha, B.H. Hameed, Adsorption of methylene blue from aqueous solution onto NaOH-modified rejected tea, Chem. Eng. J. 166 (2011) 783–786.
[65] K.A. Tan, N. Morad, T.T. Teng, I. Norli, P. Panneerselvam, Removal of cationic dye by magnetic nanoparticle (Fe_3O_4) impregnated onto activated Maize Cob Powder and kinetic study of dye waste adsorption, APCBEE Proc. 1 (2012) 83–89.
[66] R. Han, L. Zhang, C. Song, M. Zhang, H. Zhu, L. Zhang, Characterization of modified wheat straw, kinetic and equilibrium study about copper ion and methylene blue adsorption in batch mode, Carbohyd. Polym. 79 (2010) 1140–1149.
[67] R. Gong, Y. Jin, J. Chen, Y. Hu, J. Sun, Removal of basic dyes from aqueous solution by sorption on phosphoric acid modified rice straw, Dyes Pigm. 73 (2007) 332–337.